


Article

A Study on the Contact Pressure and Thermo-Elastic Behavior of a Brake Disc-Pad by Infrared Images and Finite Element Analysis

Byeong-Choon Goo 

Advanced Railroad Car Division, Korea Railroad Research Institute, 176 Cheoldobangmulgwanro, Uiwangsi, Gyeonggido 16105, Korea; bcgoo@krii.re.kr; Tel.: +82-31-460-5243

Received: 12 July 2018; Accepted: 23 August 2018; Published: 13 September 2018



Featured Application: Design and performance evaluation of disc/pad; drum/shoe; friction clutches, etc.

Abstract: To understand the tribological characteristics of a frictional brake system, it is very important to measure the contact pressure between the brake disc and pads. But until now there have been no direct methods by which to measure the contact pressure. In this study, an attempt to indirectly estimate the contact pressure is proposed. Infrared thermal images and finite element analysis were used as tools. For the thermo-elastic finite element analysis, uniform, linear, quadratic, and quartic heat flux profiles in the radial direction were applied on the disc surface. Thermal and stress fields were obtained under various conditions in the disc fixing holes and on the contact faces of the two half discs. From the numerical results, it was found that the effect of the boundary conditions on the magnitude of thermal stress was about 10%. Numerical temperature data in the radial direction could be curve-fitted to functions with the same order as the heat flux profiles. The coefficients of correlation of the curve-fittings were more than 0.91. It could be concluded that using temperature profiles obtained with an infrared camera, contact pressure distributions on the disc surface could be inferred.

Keywords: brake disc; infrared thermal image; finite element; contact pressure; temperature; thermal stress

1. Introduction

A disk brake unit stops a moving car by dissipating the kinetic energy of the car into frictional heat energy, which is generated by sliding friction between the disc and pads, when a caliper moves the brake pads into contact with the frictional surface of the disc. The contact positions and areas change during braking due to the thermo-elastic behavior of the disc and pads, the vibration of the brake unit, variation in the friction coefficient, uneven wear of the contacting surfaces, etc. Contact pressure between the two contacting surfaces also varies at every moment of the braking process. Estimating these contact positions, and pressure distribution during a braking application is a prerequisite for calculating thermal stress and designing a brake unit. In the late fifties, to obtain temperature distributions, a brake disc was modeled as a solid bound by two parallel infinite planes. A heat flux linearly decreasing with time was input to one face, while at the other face an adiabatic boundary condition was applied. To solve the one-dimensional transient heat equation, a Fourier series, the methods of images, or Laplace transform [1] was applied. Solutions showed that the disc's temperature rise was linearly proportional to the heat flux input. In the 2000s 2-dimensional transient heat problems for ideal brake discs were solved analytically by using Green's function [2] or Duhamel's integral [3]. Though the discs used in their models were similar to commercial brake

discs, the mounting seat and bolts were not included. More realistic 3-dimensional transient heat problems have been conducted using finite element analysis. One of the main merits of finite element analysis is that it can easily reflect non-linear physical or/and mechanical properties in simulation. Yevtushenko et al. [4–7] investigate the influence of temperature dependent properties such as friction coefficient, thermal conduction coefficient, and specific heat on the temperatures and wear of brake discs. Their numerical results showed that fluctuating properties had an effect on the temperature fields and wear in the disc.

Computer enhancement has allowed researchers to deal with coupled thermo-mechanical problems. Belhocine and Bouchetara [8] first obtained heat convection coefficients on every surface of the disc by air flow analysis, then performed a thermo-mechanical coupled analysis for full and ventilated brake discs. The maximum temperature on the ventilated disc surface was higher by 60 °C at 100 km/h. Hwang and Wu [9] applied a multi-body technique and a thermo-mechanical coupled model. According to their results, there were fluctuations in temperatures and stresses in the disc. Jian and Shui [10] also performed a thermo-mechanical coupled simulation for a disc/pad unit and compared their numerical and experimental results. They showed that the two results were in good agreement, and temperatures on the disc surface fluctuated during braking. Yan et al. [11] simulated turbulent flow on a ventilated disc with cross-drilled holes using finite element analysis. The cross-drilled holes provided 15–17% higher cooling capacity. Yan et al. [12] showed that X-type cooling vanes were more efficient than conventional radial vanes, increasing cooling capacity by 18–21%. Some researchers have studied thermal fatigue in brake discs. Wu et al. [13] predicted the fatigue crack propagation of a high speed railway brake disc using an extended finite element. Kim et al. [14] showed that maximum thermal stress of the disc during a single brake application was linearly proportional to the temperature rise of the disc. They measured the temperature variation of a commercial train disc, and predicted the crack initiation life of the disc using the relation between the temperature rise and thermal stress. According to Kim et al. [15], thermal stress in the disc was very sensitive to the profile of the contact pressure distribution in the radial direction. They obtained the contact pressure by solving the contact problem between the disc and pads using finite element analysis.

In the present study, a new approach to the thermo-elastic behavior of a brake disc-pad has been applied. An infrared camera and finite element analysis were adopted as tools. Surface temperatures of a ventilated cast-iron brake disc during a single brake application were measured using an infrared camera. Considering ring shaped infrared thermal images, finite element thermo-elastic analysis was performed under various conditions. For more exact thermal stress analysis, contact conditions between the disc mounting bolts and mounting seat installed on the axle were considered. The effect of boundary conditions on stress values was examined in detail. One of the main goals of the analysis was to determine the relations between temperature profiles and heat flux input profiles in the radial direction on the disc surface. It was found that two profiles could be described as functions of the same order. It was finally shown that contact pressure between the disc and pad could be assessed using the proposed approach.

2. Tests and Modeling

2.1. Tests

Tribological tests were carried out using a brake dynamometer, which can deal with full loading and real-size brake discs for commercial rail cars. Figure 1 shows a photograph and schematic diagram of the brake dynamometer. The moment of inertia of the dynamometer flywheel was 1176 kg·m². The normal force applied to each side of the disc was 16.5 kN. The friction coefficients were measured when more than 70% of the pad surface was in contact with the disc surface through a running-in condition. The initial braking speed was 150 km/h. Figure 2 shows a cast-iron brake disc and composite brake pad used for real trains. There are two pads for each side of the disc. The disc is composed of two pieces for easy maintenance, assembly and disassembly. The two pieces are joined by two bolts shown

as in Figure 2. The disc is mounted to the seat pressed on the axle. The disc temperature was measured using K-type thermocouples located at a depth of 10 mm from the surface and mid-point in the radial direction. The initial temperature of the disc was 40 °C. An infrared camera (Model A20-M, Flir, Danderyd, Sweden) was installed at a distance of 60 cm from the surface of the disc, and thermal images were taken at 15 Hz. The brake tests were repeated 3 times under the same condition. The mean friction coefficient, μ , was obtained by measuring the tangential force and the normal force acting on the disc. The forces were measured using load cells. $\mu = 0.396$ was applied for the thermal and stress analyses below.

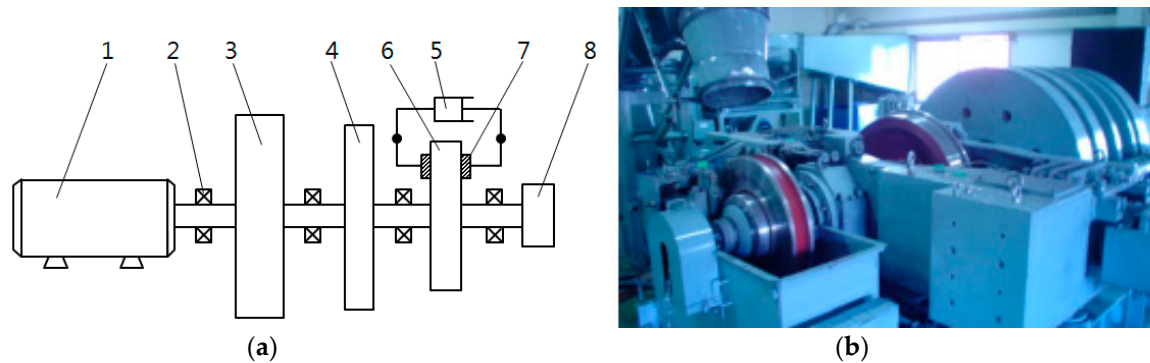


Figure 1. Brake dynamometer. 1-D.C. motor, 2-bearing, 3-Inertial wheel, 4-Tread brake, 5-air cylinder, 6-brake disc, 7-pad, 8-control box. (a) Schematic diagram; (b) Photograph.

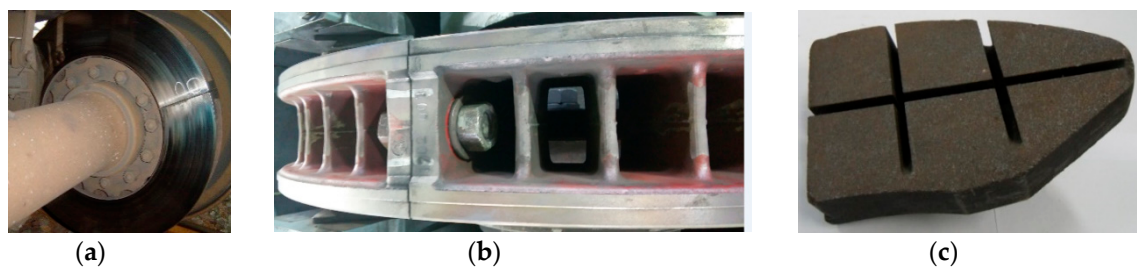


Figure 2. Ventilated cast-iron brake disc and composite brake pad used in this study. (a) Brake disc mounted to the axle; (b) Assembled brake disc; (c) Composite brake pad.

2.2. Heat Transfer

To obtain thermal fields in the disc during a stop braking, finite element analysis was carried out. When a car is decelerating from V_0 , the braking power P , is given by

$$P = Q\omega = Q(V_0 - \alpha t)/r_w \quad (1)$$

where Q is the torque applied on the disc surfaces by the brake pads, ω is the angular velocity of the axle, V_0 is the initial braking speed of the vehicle, α is the deceleration of the vehicle, and r_w is the wheel diameter of the vehicle. The torque Q , on one side of the disc is

$$Q = \int_{r_i}^{r_o} \mu p(r) 2\pi r dr \quad (2)$$

where μ is the friction coefficient between the disc and pads, and $p(r)$ is the contact pressure between the disc and pads. It is assumed that the contact pressure is uniform in the circumferential direction. This assumption is acceptable because infrared images show similar temperatures in the circumferential direction. $r_i = 195$ mm, and $r_o = 330$ mm are the inner and outer radii of the disc, respectively. During braking, some of the frictional heat is transferred to the disc, and the rest to the brake pads. The proportion of braking energy transferred to the disc, and pads can be calculated from a theoretical

solution of temperature fields for semi-infinite solids [16]. In this study, it was assumed that 90% of the frictional heat was given to the disc, and radiation heat exchange was negligible.

In this study, an isotropic and homogeneous disc was considered. And an uncoupled thermo-elastic problem was solved. The heat conduction equation and boundary conditions take the forms of Cartesian coordinates.

$$\frac{\partial^2 T}{\partial x^2} + \frac{\partial^2 T}{\partial y^2} + \frac{\partial^2 T}{\partial z^2} + \frac{\Omega}{k} = \frac{\rho c}{k} \frac{\partial T}{\partial t} \text{ in } D, t \geq 0 \quad (3)$$

$$-k \frac{\partial T}{\partial n} = q \text{ on } \Gamma_1, t \geq 0 \quad (4)$$

$$-k \frac{\partial T}{\partial n} = h(T - T_\infty) \text{ on } \Gamma_1, \Gamma_2, \Gamma_3, \Gamma_5, \Gamma_7, t \geq 0 \quad (5)$$

$$-k \frac{\partial T}{\partial n} = 0 \text{ on } \Gamma_4, \Gamma_6, t \geq 0 \quad (6)$$

$$T(x, y, z, 0) = T_0 \text{ in } D, t = 0 \quad (7)$$

where n : normal to the boundary; T_∞ : the ambient temperature; T_0 : initial temperature of the disc. The convective heat transfer coefficient, h was calculated through fluid flow analysis for a ventilated railway brake disc [9]. It can be expressed in a function of the Reynolds number, Re :

$$h = 0.6698 \frac{k_{air}}{r_0} Re^{0.6164} = 15.9219 r_0^{0.2328} w^{0.6164} \quad (8)$$

where $k_{air} = 0.025$ (W/m·°C) is the thermal conductivity of the air. All numerical analyses were performed using Abaqus (Ver. 6.16) software (Company, City, State, Country, Dassault Systèmes HQ, Waltham, MA, USA). Figure 3 shows the finite element model. The disc consisted of 407,775 quadratic tetrahedron elements. Considering the symmetry of the disc, one-fourth of the disc was included in the model. The values of the specific heat, density, thermal conductivity and thermal expansion coefficient used in the simulation were given in the function of temperatures in reference [17]. Heat flux of 40 s was given to a stop braking as shown in Figure 3. The two seconds in the beginning is the air pressure build-up time of the brake cylinder.

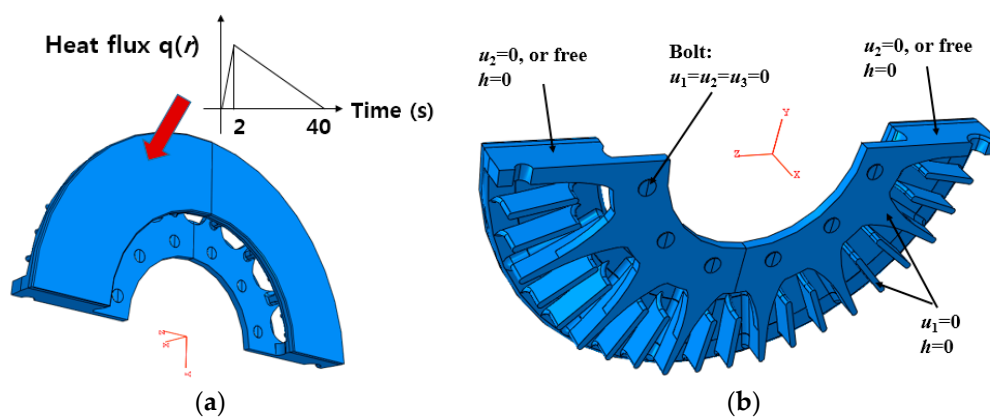


Figure 3. Finite element model and boundary conditions. (a) Heat flux; (b) Boundary conditions.

2.3. Thermoelasticity

Using the temperature fields obtained from the finite element analysis, thermal stresses were calculated from the temperature data at each time step. The same finite element model as the model used for the thermal analysis was used. But proper boundary conditions should be applied. Under the assumption of an infinitesimal displacement field $u_i(x_1, x_2, x_3)$, the thermo-elastic behavior of the

disc must satisfy the following equilibrium equations (Equation (9)), the strain-displacement relations (Equation (10)), the stress-strain relations (Equation (11)) and boundary conditions (Equation (12)):

$$\sigma_{ij,j} + X_j = 0 \text{ in } D \quad (9)$$

$$\varepsilon_{ij} = \frac{1}{2}(u_{i,j} + u_{j,i}) \text{ in } D \quad (10)$$

$$\varepsilon_{ij} = \frac{1+\nu}{E}\sigma_{ij} - \frac{\nu}{E}\delta_{kk}\delta_{ij} + \alpha_T(T - T_0) \text{ in } D \quad (11)$$

$$u_i = 0 \text{ on bolt, } \Gamma_4 \quad (12)$$

The displacement boundary conditions are shown in Figure 3. Fixed or free displacement boundary conditions were given on the two side faces of the disc (Γ_4). Mounting bolts were modeled as solid bars, and the bottoms of the bars were fixed. A frictionless condition was applied to the contact face between the bars and the bolt holes of the disc.

3. Results and Discussion

3.1. Infrared Images

Figure 4 shows the thermal images and temperature distribution along a radial line for the 2nd stop braking at 150 km/h. The initial temperature of the disc was 40 °C. In the beginning of the braking, there were three thermal bands with similar temperature levels. The temperature variation in the circumferential direction in a band was small. The maximum temperature changed from one band to another as sliding between the disc and pads progressed. But in the latter part of the braking, there was one dominant hot thermal band. This kind of phenomenon was also observed by Sawczuk [18], who measured the surface temperature of a ventilated brake disc surface using an infrared camera. In his study the initial braking speed was 200 km/h. In the beginning of braking, three rings occurred, then two rings, and finally one large ring. The contact patterns depended on the thickness of the brake pads. Figure 4 shows that the maximum temperature was around 240 °C. Some fluctuations in temperature were observed in the circumferential direction. This phenomenon can be explained easily. When a spot or band in the disc contacts the pad, the temperature of the spot increases because of frictional heat. Due to thermal expansion of the spot, the contact pressure of the spot will also increase, which will accelerate wear. After a while, the contact pressure of the spot will decrease, and the hottest spot will move to other areas of the disc. Considering the observed thermal images, four profiles of heat flux, $q(r)$: uniform, linear, quadratic, and quartic, were used in finite element analysis below.

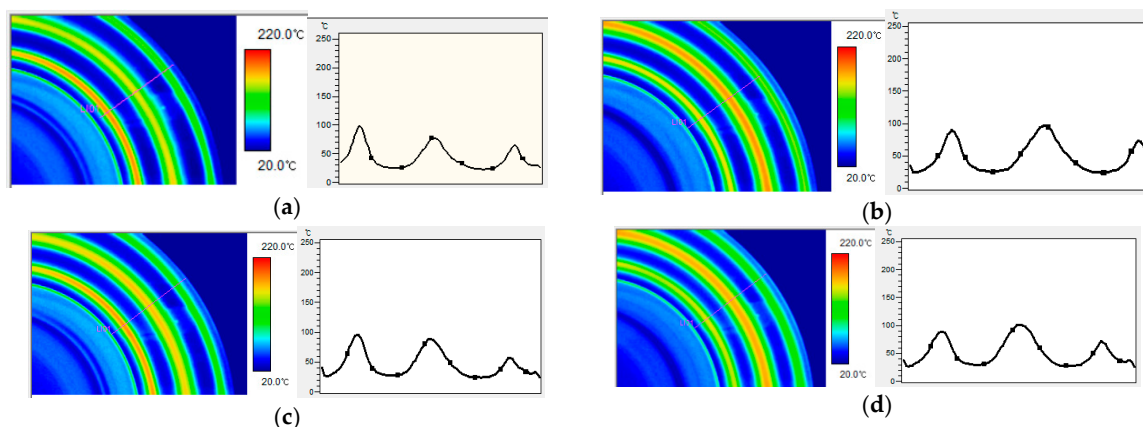


Figure 4. Cont.

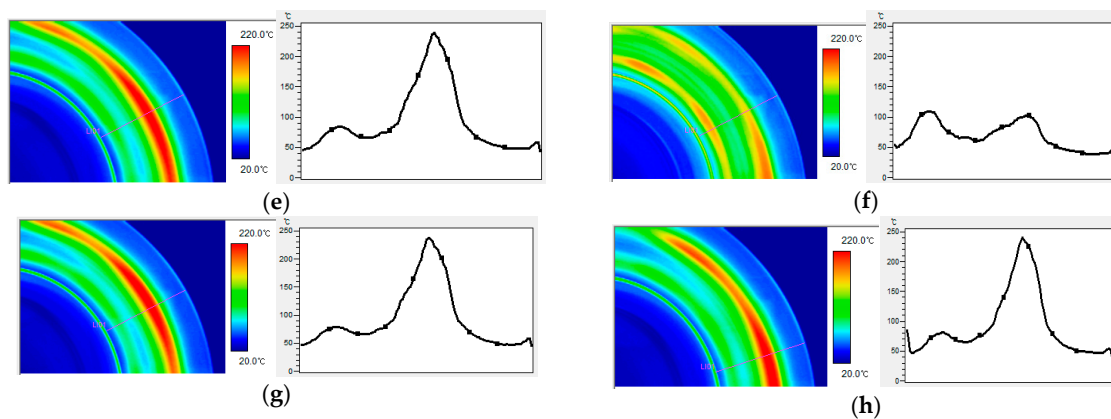


Figure 4. Infrared images of stop braking and a temperature profile along a radial line. (a) 4.805 s after brake application, (b) 6.940 s, (c) 7.341 s, (d) 8.809 s, (e) 33.634 s, (f) 34.835 s, (g) 35.502 s, (h) 36.303 s.

3.2. Finite Element Analysis

To investigate the relation between heat flux and temperature distribution in the radial direction, four types of heat flux (Figure 5) were applied on the frictional surface of the brake disc: (1) uniform distribution in the radial direction; (2) linearly increasing heat flux, which means uniform pressure in the radial direction, if the friction coefficient, μ is constant at every instant; (3) quadratic distribution; (4) quartic distribution. The total amount of heat input on the contact surface was the same for all cases.

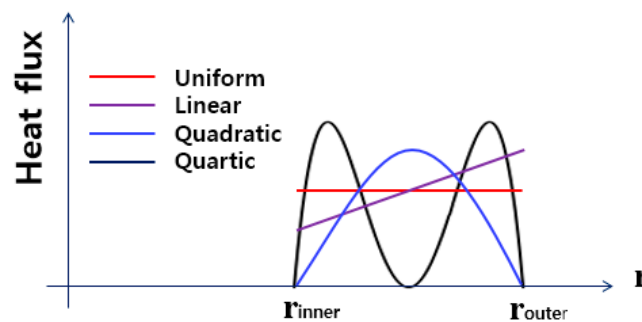


Figure 5. Four types of heat flux input in the radial direction on the brake disc surface.

Figure 6 shows the thermal and stress fields for the above-mentioned four types of heat fluxes at $t = 16.26$ s after brake application. Figure 7 represents the heat flux, temperature and stress distributions in the function of the radius on the surface of the disc. $r = 0$ and $r = 135$ are the inner and outer radii of the frictional surface of the disc. The ranges of maximum temperatures and von Mises stresses were 198–278 °C, and 165–378 MPa, respectively. The maximum temperatures and stresses along with positions on the surface are summarized in Table 1. The maximum temperature increased in the order of uniform, linear, quadratic, and quartic heat flux. In the case of the linear heat flux, the von Mises and absolute principal stress were minimum. The maximum von Mises stress and the absolute principal stress occurred in the same position except in the case of the linear heat flux. In the case of the uniform heat flux, the maximum stress occurred near the inner radius ($r = 4$). In the case of the linear heat flux, the variation in stress magnitude over the radius was not great. The results for the quadratic and quartic heat fluxes showed that the maximum stresses were generated in the middle of the heat flux bands. And the maximum stresses were greater than those for the uniform and linear heat fluxes. Therefore, in order to lower maximum thermal stress due to frictional heat, conformal contact between the disc and pads is desirable.

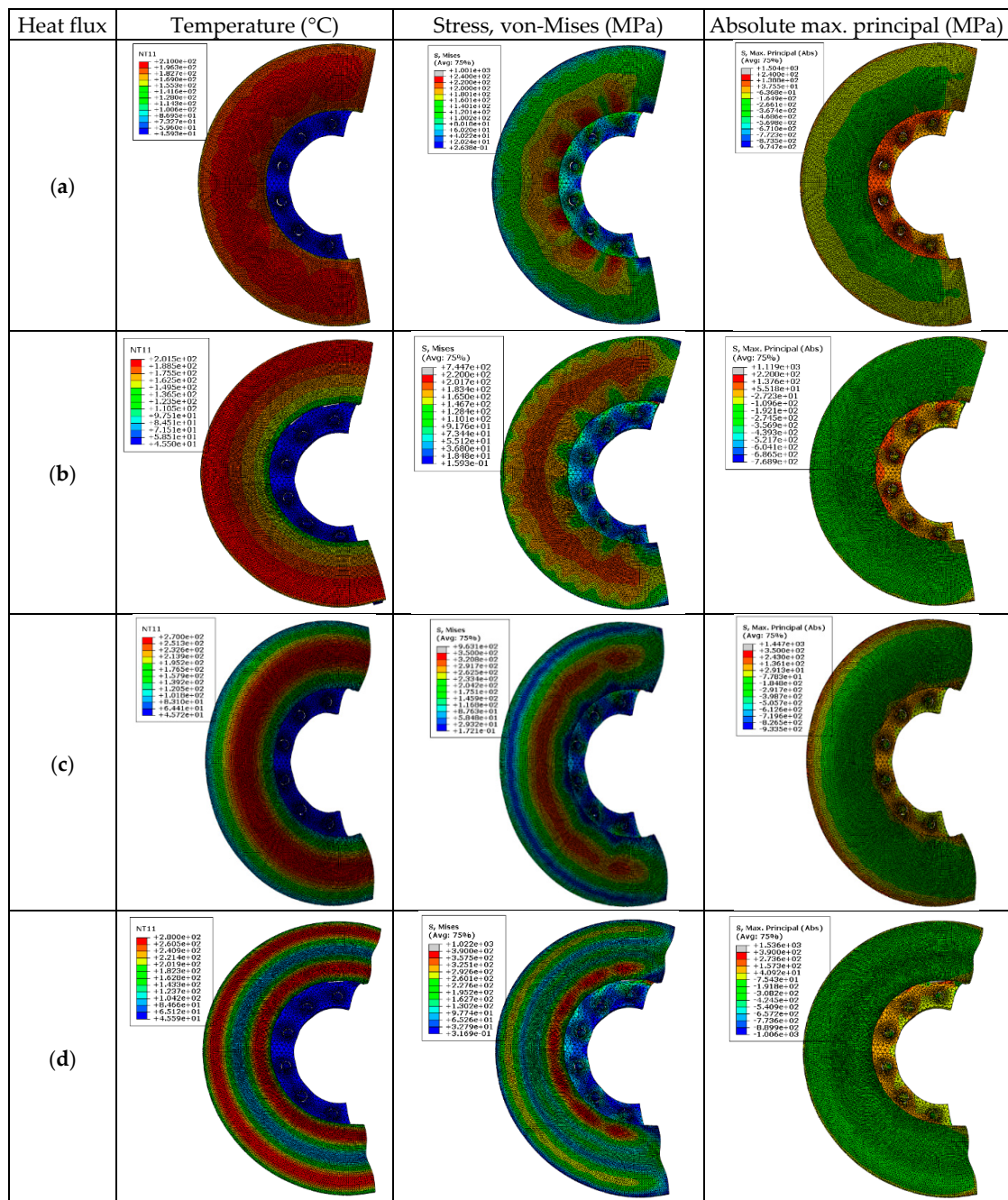


Figure 6. Thermal and stress fields at $t = 16.26$ s after brake application. (a) Uniform, (b) Linear, (c) Quadratic, (d) Quartic.

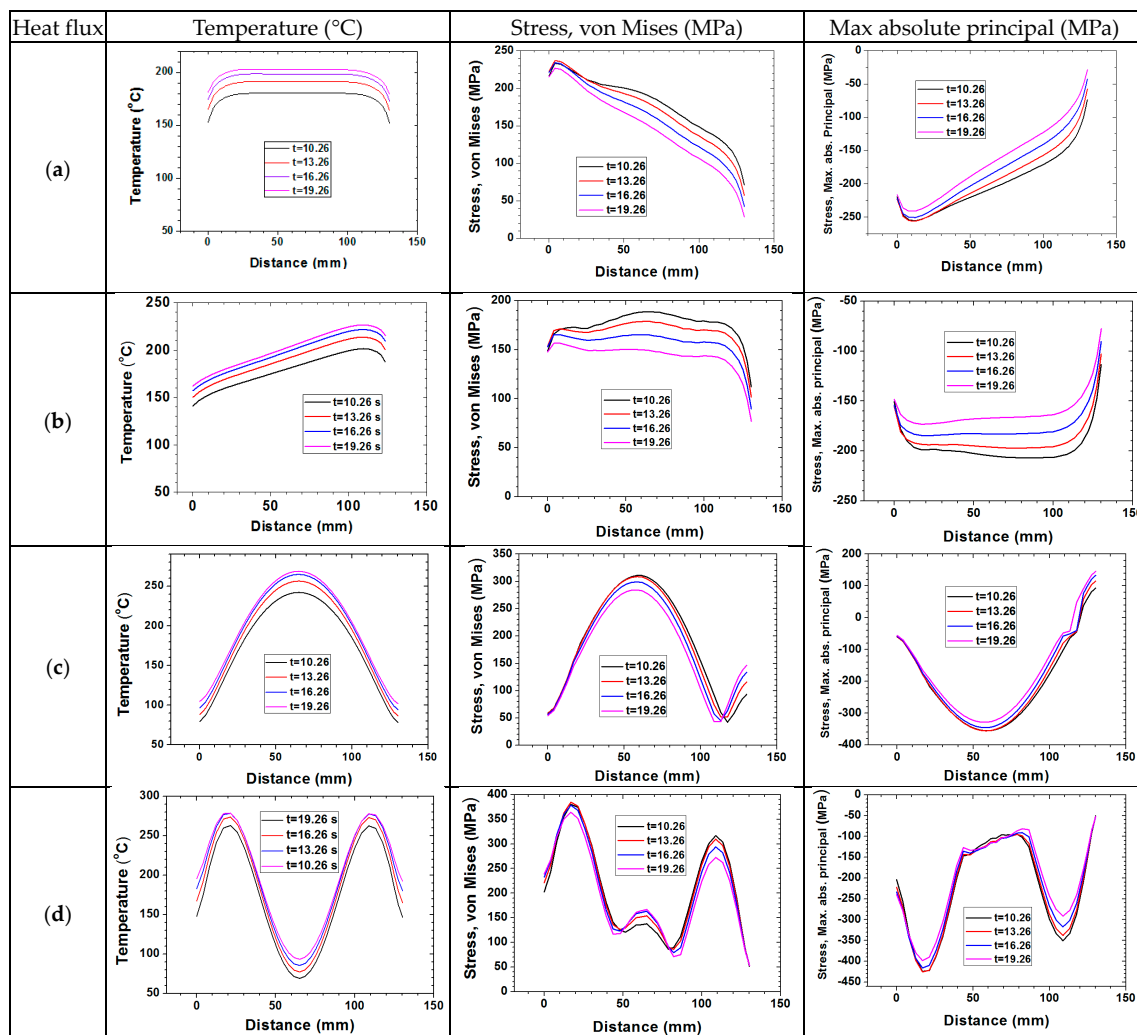


Figure 7. Comparison of temperatures, and stresses for four types of heat flux, $t = 10.26$ s. (a) Uniform, (b) Linear, (c) Quadratic, (d) Quartic.

Table 1. Maximum temperatures, positions and stresses for four types of heat fluxes at $t = 16.26$ s.

Type of Heat Flux	T_{\max} (°C)	r (mm)	Max Von Mises σ (MPa)	r (mm)	Abs. Max Principal σ (MPa)	r (mm)
Uniform	180.4	82.1	233.4	4.0	−255.4	4.0
Linear	201.5	109.3	188.8	65.1	−207.1	91.0
Quadratic	242.1	65.1	310.8	58.2	−355.3	58.2
Quartic	262.9	10.26	380.2	16.9	−424.1	16.9

Figure 8 shows the effect of boundary conditions on the stress along the symmetric line on the surface of the disc. $r = 0$ and $r = 135$ are the inner and outer radii of the frictional surface of the disc, respectively. Compared to the fixed bolt hole and fixed u_y , the u_y free condition on the sides of the disc lowered the maximum von Mises stress by 27.5 MPa (10.3%), and the bolt hole contact condition gave a 15.8 MPa (5.9%) lower von Mises stress. Applying conditions—where bolt hole contact and $u_y(u_2)$ were free, lowered the maximum von Mises stress by 31.8 MPa (11.9%). Therefore, in terms of thermal stress, a disc composed of two pieces seems to be more thermoresistant.

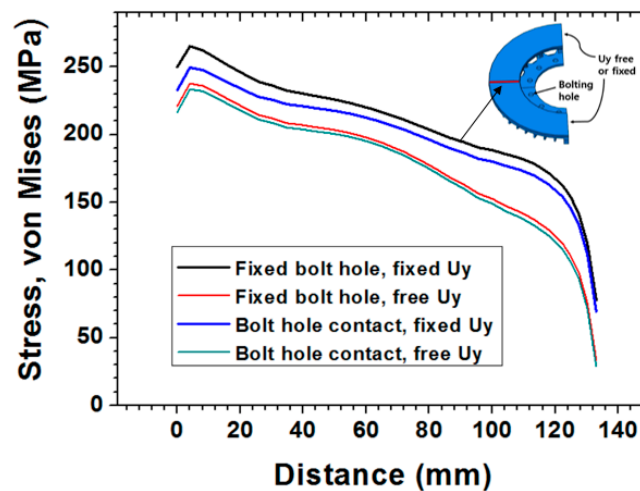


Figure 8. Stress along the symmetric line on the surface of the disc at $t = 10.26$ s under uniform heat flux.

To determine the relation between the heat flux input profiles and temperature profiles using finite element analysis, the obtained temperature data were fitted to a curve with the same order as the heat flux input. All curve fits were carried out using Excel (MS Office 2012). Figure 9 shows that the correlation coefficients, R of the curve-fitting of the temperature data were near to one, which means that the temperature and heat flux profiles have similar types of profiles. When the heat flux input was linear in the radial direction, the temperature profile was also linear. In this case the coefficients of correlation (R) were $R = 0.95$ – 0.96 . The temperature distribution was linear in the radial direction except near both edges. For quadratic heat flux, $R = 0.99$. The temperature profile in the radial direction retained a quadratic function. For the quartic heat flux input, the temperature profile maintained a quartic function. From the results it can be said that temperature profiles in the radial direction on the brake disc can be fitted by a function with the same order as the heat flux profile. Using temperature profiles of the disc surface obtained with an infrared camera, heat flux profiles can be inferred, and then pressure profiles can be estimated. [Note that heat flux = $\mu p(r)rw$.] It seems that the results of this study provide a new approach to estimating the contact pressure between brake disc and pads and for other similar cases.

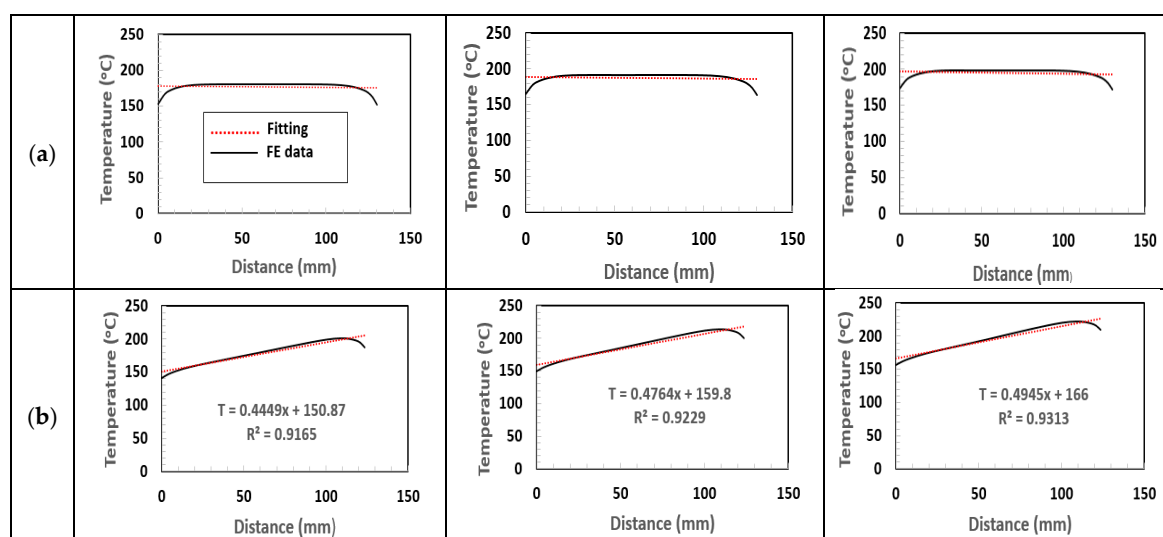


Figure 9. Cont.

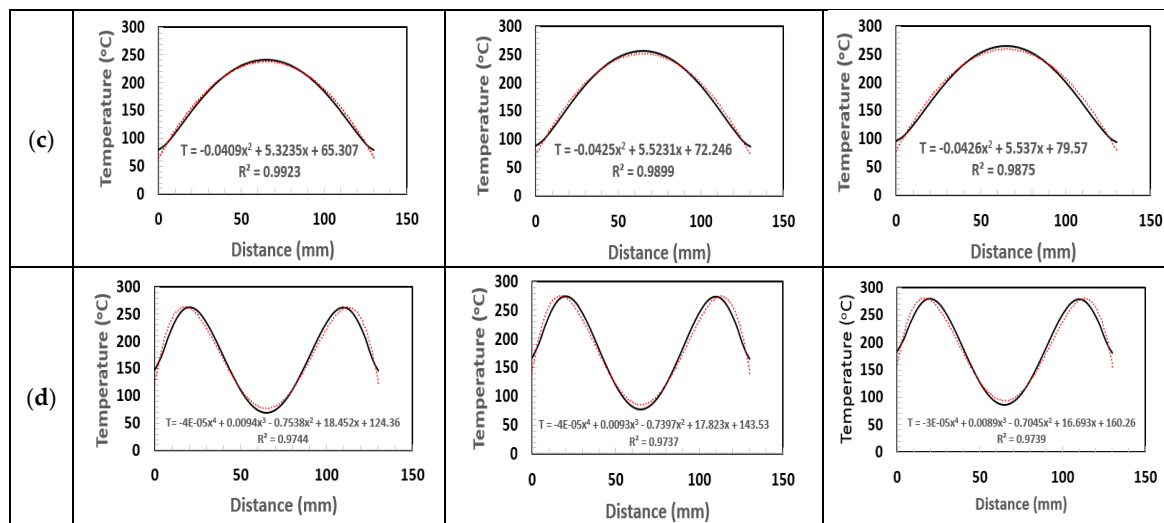


Figure 9. Curve fitting of temperature data obtained by finite element analysis. (a) Uniform, (b) Linear, (c) Quadratic, (d) Quartic.

To simulate the temperature profiles of thermal images using the process introduced above, the thermal image in Figure 4a was taken as an example. First, the temperature data of the thermal image were curve-fitted to a sixth order polynomial, $T(r)$. Figure 10a shows good correlation ($R^2 = 0.88$) between the two curves. Then the heat flux, $q(r)$, was assumed to be a similar function to $T(r)$: $q(r) = b_1[T(r) - T_b]$, where b_1 , and T_b are constants. $b_1 = 0.8$, and $T_b = 14$ were taken for the simulation. Figure 10b shows the thermal fields at $t = 4.8$ s, which are very similar to the thermal image in Figure 4a. In Figure 10c finite element temperatures in the radial direction on the surface were compared with the thermal image data. The two results were in good agreement though there was some uncertainty in the data related to the simulation. When temperature profiles cannot be represented as a polynomial, or to simulate experimental data more exactly, some coding work will be necessary. This kind of research will be pursued in the future.

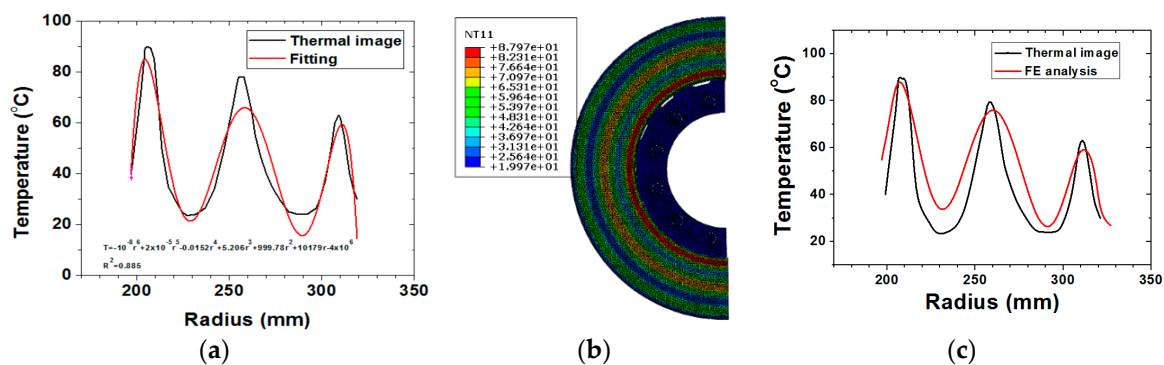


Figure 10. Comparison of thermal image temperature and finite element results. (a) Curve fitting of Figure 4a; (b) Finite element analysis; (c) Comparison of two results.

4. Conclusions

Thermal images during braking obtained with an infrared camera showed that contact between the disc and pads was not conformal. Two or three circumferential thermal bands were observed. According to thermo-elastic finite element analyses under various boundary conditions, the maximum temperature was 198–278 °C, and the thermal stress was 165–378 MPa when the initial braking speed was 150 km/h. The effect of the boundary conditions on the magnitude of stress was about 10%. Temperature profiles by curve-fitting in the radial direction resembled the heat flux profiles applied using uniform, linear, quadratic, and quartic functions along the radius. The coefficients of correlation

(R) of curve-fitting were $R = 0.95$ for the linear heat flux, and $R = 0.99$ for the quadratic and quartic heat fluxes. Using the approach provided in this study, contact pressure profiles could be inferred from the temperature profiles obtained from thermal images. It seems that the proposed method presents an insight into the study of tribology.

Acknowledgments: The author is grateful to the Korea Railroad Research Institute for the support of this research.

Funding: This study was funded by Korean Ministry of Science and ICT.

Conflicts of Interest: The author declares no conflict of interest.

List of symbols

C	Specific heat, $J/kg \cdot ^\circ C$
D	Body of the disc
E	Young's modulus, N/m^2
h	Convective heat transfer coefficient, $W/m^2 \cdot ^\circ C$
k	Thermal conductivity of the disc, $W/m \cdot ^\circ C$
n	Normal to the boundary
P	Braking power, W
q	Heat flux, W/m^2
Q	Torque on the disc surfaces by the brake pads, $N \cdot m$
t	Time, s
u_i	Component of displacement vector, m
V_0	Velocity at beginning of braking, m/s
Re	Reynolds number
r_i	Inner radius of the disc, m
r_o	Outer radius of the disc, m
r_w	Wheel diameter of the vehicle, m
T	Temperature, $^\circ C$
T_∞	Ambient temperature, $^\circ C$
X_i	Component of body force per unit volume, N/m^3

Greek symbols

α	Deceleration of the vehicle, m/s^2
α_T	Thermal expansion coefficient, $/^\circ C$
Γ	Boundary of the disc
δ_{ij}	Kronecker delta
ε_{ij}	Component of strain tensor in the Cartesian coordinates
μ	Coefficient of friction
ν	Poisson's ratio
ρ	Density, kg/m^3
σ_{ij}	Component of Cauchy stress tensor in the Cartesian coordinates, N/m^2
ω	Angular velocity of the axle, rad/s
Ω	Internal heat generation rate per unit volume, $W/s \cdot m^3$

References

1. Newcomb, T.P. Transient temperatures in brake drums and linings. *Proc. Inst. Mech. Eng. Automob. Div.* **1958**, *7*, 227–244. [\[CrossRef\]](#)
2. Talati, F.; Jalalifar, S. Analysis of heat conduction in a disc brake system. *Heat Mass Transf.* **2009**, *45*, 1047–1059. [\[CrossRef\]](#)
3. Modanloo, A.; Talaei, M.R. Analytical thermal analysis of advanced disc brake in high speed vehicles. *Mech. Adv. Mater. Struct.* **2018**. [\[CrossRef\]](#)

4. Yevtushenko, A.A.; Grzes, P. Axisymmetric FEA of temperature in a pad/disc brake system at temperature-dependent coefficients of friction and wear. *Int. Commun. Heat Mass Transf.* **2012**, *39*, 1045–1053. [[CrossRef](#)]
5. Yevtushenko, A.A.; Adamowicz, A.; Grzes, P. Three-dimensional FE model for the calculation of temperature of a disc brake at temperature-dependent coefficients of friction. *Int. Commun. Heat Mass Transf.* **2013**, *42*, 18–24. [[CrossRef](#)]
6. Yevtushenko, A.A.; Kuciej, M.; Och, E. Influence of thermal sensitivity of the pad and disk materials on the temperature during braking. *Int. Commun. Heat Mass Transf.* **2014**, *55*, 84–92. [[CrossRef](#)]
7. Yevtushenko, A.A.; Grzes, P. 3D FE model of frictional heating and wear with a mutual influence of the sliding velocity and temperature in a disc brake. *Int. Commun. Heat Mass Transf.* **2015**, *62*, 37–44. [[CrossRef](#)]
8. Belhocine, A.; Bouchetara, M. Investigation of temperature and thermal stress in ventilated disc brake based on 3D thermomechanical coupling mode. *Ain Shams Eng.* **2013**, *4*, 475–483. [[CrossRef](#)]
9. Hwang, P.; Wu, X. Investigation of temperature and thermal stress in ventilated disc brake based on 3D thermo-mechanical coupling model. *J. Mech. Sci. Technol.* **2010**, *24*, 81–84. [[CrossRef](#)]
10. Jian, Q.; Shui, Y. Numerical and experimental analysis of transient temperature field of ventilated disc brake under the condition of hard braking. *Int. J. Therm. Sci.* **2017**, *122*, 115–123. [[CrossRef](#)]
11. Yan, H.; Feng, S.; Lu, T.; Xie, G. Experimental and numerical study of turbulent flow and enhanced heat transfer by cross-drilled holes in a pin-finned brake disc. *Int. J. Therm. Sci.* **2017**, *118*, 355–366. [[CrossRef](#)]
12. Yan, H.B.; Zhang, Q.C.; Lu, T.J. Heat transfer enhancement by X-type lattice in ventilated brake disc. *Int. J. Therm. Sci.* **2016**, *107*, 39–55. [[CrossRef](#)]
13. Wu, S.C.; Zhang, S.Q.; Sun, Q.D.; Jiang, C.S.; Xu, Z.W. Thermal crack growth-based fatigue life prediction due to braking for a high-speed railway brake disc. *Int. J. Fatigue* **2016**, *87*, 359–369. [[CrossRef](#)]
14. Kim, D.J.; Seok, C.S.; Koo, J.M.; We, W.T.; Goo, B.C.; Won, J.I. Fatigue life assessment for brake disc of railway vehicle. *Fatigue Fract. Eng. Mater. Struct.* **2010**, *33*, 37–42. [[CrossRef](#)]
15. Kim, D.J.; Lee, Y.M.; Park, J.S.; Seok, C.S. Thermal stress analysis for a disc brake of railway vehicles with consideration of the pressure distribution on a frictional surface. *Mater. Sci. Eng. A* **2008**, *483–484*, 456–459. [[CrossRef](#)]
16. Newcomb, T.P. Determination of the area of friction surfaces of automotive vehicles. *J. Mech. Eng. Sci.* **1960**, *2*, 312–324. [[CrossRef](#)]
17. Lim, C.H.; Goo, B.C. Development of compacted vermicular graphite cast iron for railway brake discs. *Met. Mater. Int.* **2011**, *17*, 199–205. [[CrossRef](#)]
18. Sawczuk, W. The evaluation of a rail disc braking process by using a thermal camera. *Meas. Autom. Monit.* **2015**, *61*, 265–270.

